Digest Journal of Nanomaterials and Biostructures Vol. 10, No. 3, July - September 2015, p. 1043 - 1053

PURE AND RARE EARTH DOPED COBALT FERRITE LASER ABLATION: SPACE AND TIME RESOLVED OPTICAL EMISSION SPECTROSCOPY

G. BULAI[a*], S. GURLUI[a], O. F. CALTUN[a], C. FOCSA[b]
[a]*Faculty of Physics, Alexandru Ioan Cuza University of Iasi, 700506 Iasi, Romania*
[b]*Laboratoire de Physique des Lasers, Atomes et Molécules (UMR CNRS 8523), Université de Lille 1 Sciences et Technologies, 59655 Villeneuve d'Ascq cedex, France*

Cobalt ferrite thin films with preferential crystallographic structure, controlled composition and perpendicular magnetic anisotropy can be obtained by pulsed laser deposition. Their properties are influenced by the experimental conditions and thus by the deposition plasma plume characteristics. The aim of this study was to obtain information on the dynamics of the expanding plasma generated by laser irradiation (532nm, 10 ns, 10Hz) of three bulk materials of pure and rare-earth doped (RE=Dy, Gd) cobalt ferrite. This was done through space- and time-resolved optical emission spectroscopy using an ICCD camera and a monochromator. Both the global dynamics of the plasma and the evolution of individual species were analyzed. From the space- and time-evolution of several spectral lines, we determined the velocities of the main plasma plume constituents. The excitation temperature spatial distribution was obtained from the Boltzmann plot of four spectral lines, in the assumption of local thermodynamic equilibrium.

(Received July 15, 2015; Accepted September 8, 2015)

Keywords: Cobalt ferrite; Rare earth; Laser ablation; Plasma dynamics; Excitation temperature.

1. Introduction

Magnetic materials are the focus of many researches due to their potential applications in various technology fields. Among these, cobalt ferrite is a spinel ferrimagnetic material with high coercivity, moderate saturation magnetization, high magnetocrystalline anisotropy and large magnetostrictive effect [1,2]. In nano-scale structures, this material presents a higher interest due to the possible applications in miniaturized data storage devices, sensors, actuators and waveguides. Significant advances have been made in nanotechnology not only through chemical routes (such as sol-gel [3], spin-spray [4], polymer precursor method [5]), but through physical methods as well (e.g.: magnetron sputtering [6], molecular beam epitaxy [7]). Cobalt ferrite thin films with specific properties such as preferential crystallographic structure [8], uniform chemical distribution and perpendicular magnetic anisotropy [9] were obtained by Pulsed Laser Deposition (PLD) [2, 10].

A detailed analysis on the structural, magnetic and dielectric properties of the bulk materials used in this study as targets is reported in [11]. Both XRD and Raman spectroscopy measurements indicated the presence of a second orthoferrite phase for the RE doped cobalt ferrite samples. The density values obtained for the doped materials were lower than that of the stoichiometric cobalt ferrite. Moreover, the thin films deposited by pulsed laser deposition using these targets as source materials presented a decreased crystallinity for the RE doped cobalt ferrite films compared to the un-doped samples, although deposited in the same conditions and even when using a 400^{o}C *in-situ* substrate heating [9]. Considering that the inclusion of RE elements induced changes in structural and magnetic characteristics of the bulk materials and of the

* Corresponding author: georgiana.bulai@uaic.ro

deposited thin films one could also expect an influence on the dynamics of the laser induced plasma plume.

Within this framework, the ablation plasma plume analysis can provide valuable information to be used in explaining the structural and chemical properties of the deposited nano-structured materials and also in optimizing the deposition process itself. For instance, Mukherjee et al. [10] obtained highly textured cobalt ferrite thin films on silicon substrate by oblique-angle pulsed laser deposition and concluded that the spatial expansion of the plume with respect to the substrate tilt angle was very important when optimizing the growth process in order to obtain uniform thin films with smooth surface morphology. In another study on PZT ($PbZr_{0.52}Ti_{0.48}O_3$) the same authors revealed (by ICCD imaging of the ablation plasma plume) that the axial dimension (perpendicular to target surface) of the plume increased significantly as the fluence was increased from 1 to 3 J/cm^2 [12]. The more intense signal of the ICCD image recorded for 3J/cm^2 suggested a higher ionization/excitation of the ejected species, which in turn led to higher crystallinity and better morphology of the deposited film. Moreover, the wider lateral expansion ensured a more uniform deposition over a larger area. In the same paper, the influence of the oxygen background pressure on the plasma plume dynamics was studied, in relation with the growth of multilayered structures of PZT and $La_{0.7}Sr_{0.3}MnO_3$ (LSMO). Another study on PZT laser ablation plasma characterization was performed by Kumar et al. [13], showing that the oxygen pressure has an important influence on the time-of-flight profiles, spatial distribution of the excitation temperature and electronic density. Their paper also presented the structural characteristics of the deposited film which were correlated to the pressure used during the film growth. All these examples highlight the importance of the laser ablation plasma plume dynamics and energetics analysis and of the expected correlations with the properties of the target bulk material and deposited thin films.

In this paper, we investigate for the first time the properties of plasma plumes generated by laser ablation (in PLD configuration) of one of the most promising magnetic materials: cobalt ferrite, pure ($CoFe_2O_4$) or doped with Dy ($CoFe_{1.8}Dy_{0.2}O_4$) or Gd ($CoFe_{1.8}Gd_{0.2}O_4$). This work continues a series of similar studies on other types of materials with different chemical compositions, from the simplest ones (Al [13], Al_2O_3 [14])) to more complex systems (As_xSe_{100-x} [15], GaLaS [16], $BNSiO_2$ [17]).

2. Experimental details

The experimental set-up (Figure 1) consists of a stainless steel vacuum chamber, equipped with a dry pump (Agilent Technologies TS-300) which can ensure a 10^{-2} Torr pressure. A thorough description of the experimental set-up and of the acquisition method is given in [16]. The cobalt ferrite target was placed on a micrometric precision 3D translation stage. The second harmonic of an Nd-YAG laser (Quantel Brilliant, 532 nm wavelength, 10 ns pulse duration, 10 Hz repetition rate) was focused at normal incidence on the target by a 25 cm focal length lens. The estimated impact area was 0.5 mm^2 while the laser energy was set at 50 mJ which led to a fluence of 10 J/cm^2. The laser characteristics were the same as those used for thin film deposition from the same targets [9]. The plasma plume analysis was done using an ICCD PI-MAX camera (PIMAX2-91003-UNIGEN2, 1024 × 1024 pixels, minimum gating time 2 ns) connected with high resolution monochromator (Acton SP2500i, 500 mm focal length) fitted with one mirror and two diffraction gratings (300 lines/mm, 2400 lines/mm) mounted on the same three-position turret [17].

The investigation of the plasma global dynamics was done by analyzing sequential snapshots taken at different delays with respect to the laser pulse. These images were recorded using the mirror position of the monochromatic turret and a low value of 5ns ICCD gate time for a higher temporal resolution of the expansion process. For spectroscopic analysis the monochromator 2400 lines/mm diffraction grating was used. First, optical emission spectra over 300 nm – 550 nm spectral range were recorded using an ICCD gate time of 5 μs to obtain a global overview of all the species present in the plasma. Once identified, space – and time – resolved optical emission analysis was done on several selected lines, using narrower spectral ranges (~7nm). The spatial distribution of the line intensity was achieved by placing a 1mmx5mm slit on

the optical path between the plume and the monochromator, thus analyzing only a 0.1 mm wide plasma slice, as indicated in Figure 1.

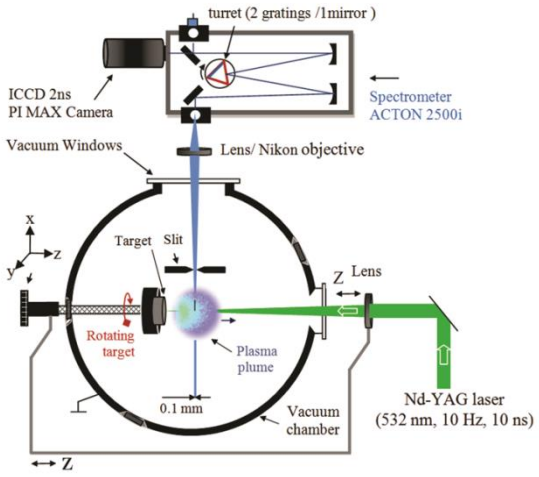

Fig. 1. Schematic view of the experimental set-up used for laser ablation plasma characterization

The $CoFe_{1.8}RE_{0.2}O_4$ bulk materials were obtained by standard ceramic technique using powder oxides of the constituent elements (Fe_2O_3, Co_3O_4 and $La_2O_3/Dy_2O_3/Gd_2O_3$) as starting materials mixed in adequate proportions. The intermediate steps of the synthesis process were described in [11]. The powders were wet mixed, dried and calcined in air at 950^{o}C for 5 h and then ball milled for 8 h. Finally the milled powders were sintered at 1250^{o}C for 5 h. The stoichiometric cobalt ferrite target was sintered in the same conditions as the doped materials.

3. Results and discussions

3.1 ICCD imaging – optical diagnostics

An initial step in analyzing the properties and dynamics of the laser induced plasma was to study its non-dispersed optical emission. Figure 2 presents as an example various snapshots of the Gd-doped cobalt ferrite plasma plume taken with the ICCD camera at various delays with respect to the laser pulse. In order to catch the finest details in the dynamics of the plasma plume «as a whole», we used a very low value for the ICCD gate (5 ns), which ensured a reasonable contrast of the pictures up to ~500 ns and plume spatial extension of ~4 cm (see Figure 2). We note that this is in range with typical target-substrate distances (a few cm) used in actual PLD experiments on the same materials [8,9]. For all three types of targets, the ICCD images revealed the presence of two structures with distinct dynamics in the plume. To determine the "center-of-mass" velocity of these two structures, we plotted the distance from the target of the highest intensity emitting point (in each structure) versus the time at which the snapshot was taken. The velocities are derived from the slope of the linear fit of this dependence and are listed in Table 1.

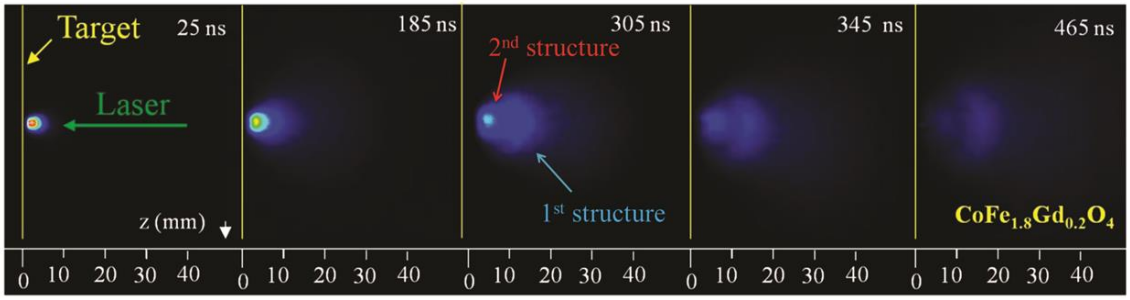

Fig. 2. Temporal evolution of the Gd-doped cobalt ferrite plasma plume emission (5 ns ICCD gate time)

Table 1. Center-of-mass (COM) velocities of the two main structures observed from the ICCD imaging of the three plasma plumes studied

Sample	**Velocity of the first structure (10^3 m/s)**	**Velocity of the second structure (10^3 m/s)**
$CoFe_2O_4$	10.7 (±0.7)	2 (±0.15)
$CoFe_{1.8}Dy_{0.2}O_4$	9.2 (±0.5)	2.3 (±0.17)
$CoFe_{1.8}Gd_{0.2}O_4$	8 (±0.3)	2.6 (±0.09)

The first structure displays velocity values five times higher than the second one which is closer to the target surface. This splitting process was observed in our previous works (both by experimental [13,14,18] and theoretical approaches [19, 20]) and in the results reported by other research groups [21,22]. Despite the low amount of RE elements (RE:Fe = 1:9), it seems that this is enough to induce a small variation of the COM velocities on both structures. While the second structure (the one closest to the target) presents slightly increased velocities for the RE-doped samples, the first structure (fast component) of the RE containing ferrite plasmas have lower velocity values than the stoichiometric cobalt ferrite. These different dynamics could also be related to the differences in the density of the bulk material (5.19g/cm^3 - $CoFe_2O_4$, 3.81g/cm^3 - $CoFe_{1.8}Dy_{0.2}O_4$, 4.05g/cm^3 - $CoFe_{1.8}Gd_{0.2}O_4$) and to the physical characteristics of the main elements (atomic mass, ionic radius). While the increase of the second structure velocity is more influenced by the lower density of the RE doped bulk samples, the velocity of the first plasma plume structure is reduced due to the much larger mass of the RE elements compared to Co and Fe. More information on the nature and properties of the two structures was obtained by studying the spatial and temporal profiles of the spectral line intensities acquired through optical emission spectroscopy.

3.2 Space and time resolved optical emission spectroscopy

The ICCD imaging results offer a global view of the plasma plume dynamics, however further investigations should be done in order to determine the contribution of each species and of other parameters which can give more information on the processes that take place in plasma plume formation and expansion. With this purpose we performed a spatio-temporal resolved spectroscopy study by analyzing the spectral lines of ions and neutrals at different delays from the laser pulse and at different distances from the target surface. First, optical emission spectra in the 300 nm – 550 nm range were recorded using a 5μs ICCD gate width so as to detect as many species as possible.

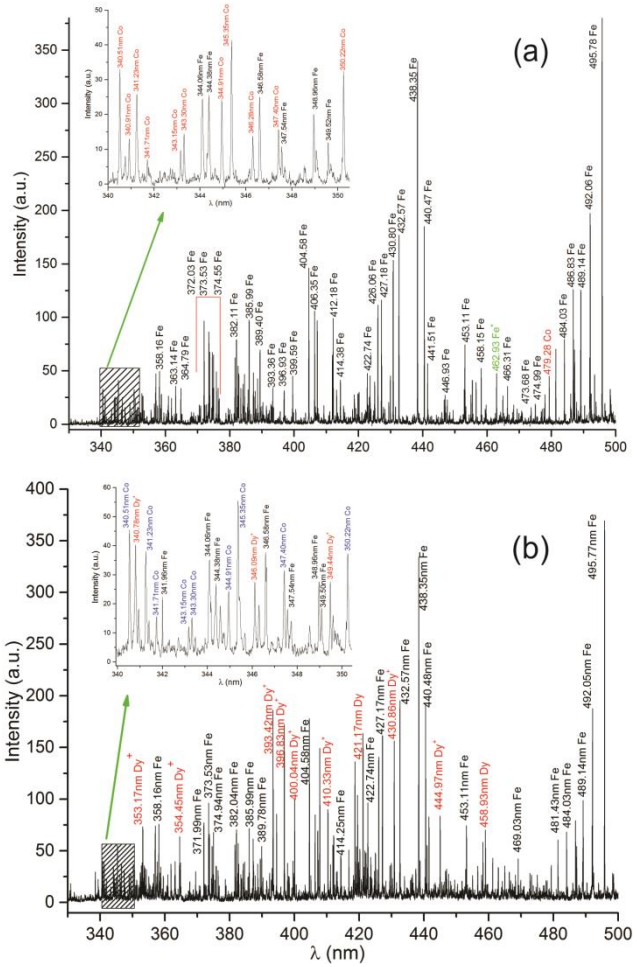

Fig. 3. Optical emission spectra of 0.1 mm wide plasma slice located in the immediate vicinity of the target for $CoFe_2O_4$ (a) and $CoFe_{1.8}Dy_{0.2}O_4$ (b) ablation (ICCD gate time - 5 μs, gate delay - 25 ns)

Fig. 3 presents the spectral lines observed in this wavelength range for the cobalt ferrite and Dy doped cobalt ferrite laser induced plasmas. The presence of both cobalt and iron species was confirmed by identifying the recorded lines for the cobalt ferrite plasma using the available databases [23,24]. For a clearer presentation, in Fig. 3 (a) only the most intense spectral lines were indexed which in most cases were associated with iron species transitions. In order to show also the presence of Co neutrals, a zoom of the 340 nm – 350 nm region is presented in the inset of this Figure. The presence of more lines corresponding to iron transitions is justified by the higher concentration of Fe compared to Co (Fe:Co - 2:1) and by its richer emission spectrum. Moreover, no clear assignment of the observed spectral lines with the oxygen related transitions were made due to their much lower intensity compared to iron and cobalt emission lines as observed from the available database [23]. For the Dy doped cobalt ferrite plasma, beside the Fe and Co spectral lines, one can also observe the presence of Dy ion transitions, although its concentration is much smaller than the ones of the main elements. This can be tentatively explained by the lower ionization potential of Dy (5.93 eV) compared to Fe and Co.

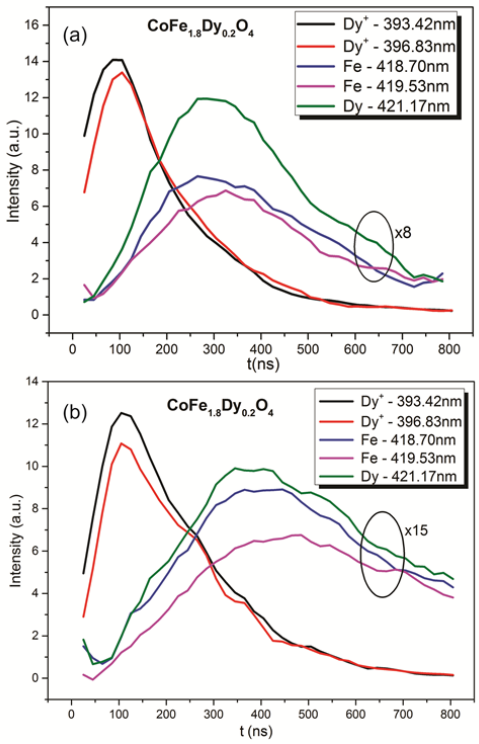

Fig. 4. Temporal profiles of several spectral lines observed for the Dy-doped cobalt ferrite plasma slice (0.1 mm wide) centered at distance of 1.2 mm (a) and 1.9 mm (b) from the target surface and recorded using a 50ns ICCD gate width. Multiplicative factors were applied to the neutrals signal for better visibility

Once the observed spectral lines were identified, further space- and time- resolved emission spectroscopy analysis was done on several selected species in the narrower spectral ranges of interest. For velocity calculations, optical emission time-of-flight profiles (such as those shown in Figure 4 for Dy-doped cobalt ferrite plasma plume) were recorded for various neutral and ionic spectral lines at different distances from the target surface using a 50 ns ICCD gate width. The temporal distributions were smoothened and the intensity values of the neutral species recorded at the 0.5 mm and 1.9 mm distances were multiplied (for better visibility) by a factor of 8 and 15, respectively. In both cases, the maximum intensity of the temporal distribution for ions was recorded at lower delays than the one corresponding to neutral species. This observation indicated a higher velocity for ions than for neutrals. Moreover, as the distance increases, the maximum values of the ion profiles present a smaller temporal shift (from 90 ns at 0.5 mm to 110 ns at 1.9 mm) than the ones of the neutral species (from 320 ns at 0.5 mm to ~390 ns at 1.9 mm), indicating a higher velocity for the rare-earth ions.

The axial velocities of the investigated species were determined from the slope of the linear plot of the dependence between the distance and the delay at which the maximum intensity was observed. Figure 5 presents an example of this type of dependence obtained for the Dy^+ ion while the as-obtained axial velocities of several species present in the investigated plasmas are listed in Table 2. The calculated velocity error bars for the analyzed species were ~0.5 km/s. As one can observe, these results reveal the presence of two groups with distinct dynamics: one formed by neutrals with velocities in the range of 1 to $3 \cdot 10^3$ m/s ("slow" structure) and a second one which consists mainly in ionic species with velocities of almost one order of magnitude higher than the previous one ("fast" structure).

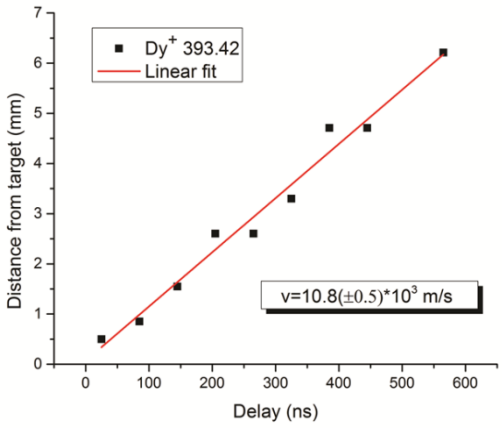

Fig. 5. Dy^+ axial velocity derived from the space- and time-evolution of the 393.42 nm spectral line intensity

Table 2. Velocities of several species present in the plasma, derived from the space- and time-evolution of the spectral lines intensities

$CoFe_2O_4$		$CoFe_{1.8}Dy_{0.2}O_4$		$CoFe_{1.8}Gd_{0.2}O_4$	
Element	**Velocity (10^3 m/s)**	**Element**	**Velocity (10^3 m/s)**	**Element**	**Velocity (10^3 m/s)**
Fe (404.58nm)	2.5	Fe (419.53nm)	2.1	Fe (404.58nm)	3.3
Fe (406.35nm)	2.1	Fe (418.7nm)	1.9	Fe (532.41nm)	2.1
		Fe (426.04nm)	1.7	Fe (535.33nm)	2.4
		Dy (421.17nm)	1.5	Gd (534.3nm)	1.8
		Dy^+ (393.42nm)	10.8	Gd^+ (406.35nm)	11.1
		Dy^+ (396.83nm)	9.0	Gd^+ (404.98nm)	13.0
				Gd^+ (409.86nm)	12.3

The existence of two structures formed by different types of species can be explained on the basis of two distinct ejection mechanisms which are described in our previous papers [13]: one based on electrostatic repulsion and another one linked to thermal mechanisms. At very short time scale, the very intense field left by electron laser excitation and detachment determines the ejection of the ions through a Coulomb process. As electrons are removed from the surface, the induced net positive charge accelerates the positive ions away from the surface depending on their mass and ionization degree. In the case of nanosecond laser ablation, the energy of the incident radiation is transmitted to the crystalline lattice of the bulk materials which determines the heating, melting and then vaporization of the solid. The neutrals, which present lower velocities, are generated by thermal processes that take place at higher delays with respect to the laser pulse.

3.3 Excitation temperature profiles

To obtain more information about the properties of the laser induced plasma we calculated the excitation temperatures of several species at various distances from the target surface using the

Boltzmann plot method. Briefly, the intensity of a given spectral line (arising from the transition between the upper energy level *k* and the lower energy level *i*) is written as:

$$I_{ki} = \frac{A_{ki}}{\lambda_{ki}} g_k Z(T) \exp\left(-\frac{E_k}{k_B T}\right) \quad (1)$$

where A_{ki} and g_k are the transition probability between level k and level i and statistical weight of level k, Z(T) is the partition function, λ_{ki}, E_k, k_B and T are the wavelength, energy of level k, Boltzmann constant and excitation temperature, respectively. The excitation temperature value is then calculated as the slope of the linear dependence $\ln\left(\frac{I_{ki}\lambda_{ki}}{g_k A_{ki}}\right) = f\left(E_k\right)$

This calculation method can be applied in the assumption of a local thermodynamic equilibrium (LTE). Usually this condition is verified by the McWhirter criterion [25], which relates the electron number density and temperature. However, the use of this criterion was recently subject to serious questioning [26]. Here we propose an alternative approach to check the existence of the LTE in the plasma (already used in previous work [13]). Briefly, we use two spectral lines arising from the same upper level, which cancels the influence of the temperature in their intensity ratio. From the experimental data, we calculate then the $A_{ki} \cdot g_k$ product and compared it with available database values. For instance, when considering the first two Fe lines from Table 3, one gets an experimental value of $2.15 \cdot 10^8$ s^{-1}, to be compared with the database value of $2.13 \cdot 10^8$ s^{-1} [23]. The excellent agreement between these two values is, in our opinion, an argument for the existence of the LTE in our plasma. .

In this study, for excitation temperature (T_e) calculation we considered four Fe spectral lines with the same lower energy level (last four lines in Table 3). The same four lines were considered in T_e calculation of all three laser induced plasma plumes (pure and rare earth doped cobalt ferrite).

Table 3. Spectroscopic parameters of Fe spectral lines considered in the analysis

Wavelength (nm)	**A_{ki} (s^{-1})**	**g_i - g_k**	**E_{upper} (eV)**	**E_{lower} (eV)**
500.61	5.87E6	11 - 11	5.308	2.832
523.29	1.94E7	9 - 11	5.308	2.939
404.58	8.62E7	9 - 9	4.548	1.484
438.35	5E7	9 - 11	4.312	
516.74	2.72E6	9 - 7	3.883	
427.17	2.28E7	9 - 11	4.386	

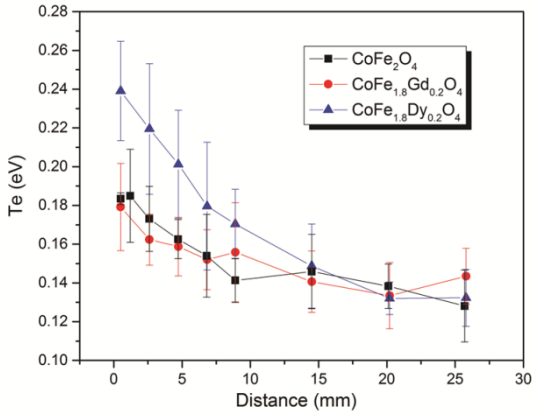

Fig. 6. Excitation temperature variation with distance from the target surface for Fe in the three laser ablation plasmas

The behavior of the excitation temperature was studied as a function of the distance from the target surface. Fig. 6 presents this variation for the Fe neutral in the three types of laser induced plasmas (pure and rare earth doped cobalt ferrite plasma). The error bars were calculated from the linear fit standard deviation of the $\ln\left(\frac{I_{ki}\lambda_{ki}}{g_k A_{ki}}\right) = f\left(E_k\right)$ dependence. In all cases a decrease of the excitation temperature with distance was observed. The same behavior was reported by *Salik et al.* in their optical investigation study of iron plasma generated by nanosecond laser ablation [27]. Using the Boltzmann plot as well, *De Giacomo et al*. observed ionic and atomic temperature decrease when analyzing the TiO_2 plasma in 10^{-2} Torr oxygen pressure at 1.5 J/cm^2 fluence of a KrF excimer laser [28].

Many characteristics of Dy and Gd elements are approximately the same (e.g.: mass, ionic radius, thermal conductivity), different values being observed between their melting temperature (Gd: 1312 ^{o}C, Dy: 1407 ^{o}C) and vaporization heat (Gd: 359.4 kJ/mol, Dy: 230 kJ/mol). The optical emission spectroscopy results revealed a higher excitation temperature for the Dy-doped cobalt ferrite compared to the undoped and Gd doped plasma and lower velocities of the Dy ions and neutrals compared to those of the Gd species. At smaller distances from the target surface, a 600K electronic temperature difference between the Dy doped and Gd doped cobalt ferrite plasma was observed. Both this dependence and the velocity variations of the RE elements can be tentatively explained on the basis of the difference between the vaporization temperature of Dy and Gd. The lower evaporation heat of Dy compared to Gd means that more Dy atomic systems will pass into an excited state, thus the excitation temperature will be higher. There is also a difference between the ionization potential of the two elements (Dy: 5.93eV; Gd: 6.15eV) but its value is relatively small to explain the higher ionization degree of Dy compared to Gd species. Moreover, the higher kinetic energy of Dy right after the laser-target interaction is lost through excitation mechanisms, leading to a lower velocity for this element.

Beyond a distance of 9 mm from the target surface, regardless of the plasma composition, the excitation temperature is approximately the same. This result reveals the importance of the collision processes that take place during the plasma expansion, which lead to a thermalization of the induced plasma, even when RE elements are present. The distribution of excited species and the population of their electronic levels remain practically the same and the contribution of the RE dopants is insignificant.

While the optical emission spectroscopy revealed lower velocities for Dy species compared to Gd ones, the ICCD imagery showed higher velocities for the “fast” structure in Dy doped cobalt ferrite plasma compared to the one found in Gd doped cobalt ferrite. To explain this inconsistency one should consider that the ICCD images capture the emission of all plasma components and that the dynamics of the first structure is given not only by the RE element but

also by the Co and Fe ions. In our case, the lower intensity of the Co^+ and Fe^+ lines prevented us from getting reliable velocity values for these species.

4. Conclusions

ICCD imaging and optical emission spectroscopy analysis were used to obtain information on the dynamics of the plasma plume and of its constituents together with spatial distribution of atomic iron excitation temperature. By fast-gate ICCD imaging, two main structures with different velocities were observed. Further investigations done by space- and time-resolved spectroscopy analysis revealed that the previously observed "fast" component is mainly formed by ions, while the second one is mainly due to neutral contribution. Using Boltzmann plot, spatial profiles of neutral iron excitation temperature were plotted for all three types of bulk materials and similar dependences were observed. However, at short distances from the target surface, the excitation temperature found for the $CoFe_{1.8}Dy_{0.2}O_4$ plasma was 600K higher than the one found for $CoFe_{1.8}Gd_{0.2}O_4$. Both excitation temperature and individual velocity variations were explained on the basis of the different vaporization heat and melting temperature values of the two rare-earth elements. Further studies of the plasma plume obtained in different conditions of pressure and fluence are considered.

Acknowledgements

This work was supported by the European Social Fund in Romania, within the Managing Authority for the Sectoral Operational Programme for Human Resources Development 2007-2013 [grant POSDRU/159/1.5/S/137750], Ministry of National Education, within RO-CERN (ELI-NP; FAIR) / 21.05.2014 Program (Project ELIAN Nr. E03), Romanian National Authority for Scientific Research, CNCS-UEFISCDI, project number PN-II-ID-PCE-2011-3-0650, PHC project Brancusi Nr. 29551XB and "Alexandru Ioan Cuza" University within "UAIC Grants for young researchers" competition (project code GI-2014-06).

References

[1] S. C. Sahoo, N. Venkataramani, S. Prasad, M. Bohra, R. Krishnan, J Nanosci Nanotechnol. **10**, 3112 (2010).
[2] M. C. Terzzoli, S. Duhalde, S. Jacobo, L. Steren, C. Moina, J. Alloys Compd. **369**, 209 (2004).
[3] A. V. Raut, R. S. Barkule, D. R. Shengule, K. M. Jadhav, J. Magn. Magn. Mater. **358-359**, 87 (2014).
[4] A. A. Bagade, V. V. Ganbavle, K. Y. Rajpure, J. Mater. Eng. Perform. **23**, 2787 (2014).
[5] M. Gharagozlou, J. Alloys Compd. **486**, 660 (2009).
[6] H. Yanagihara, Y. Utsumi, T. Niizeki, J. Inoue, E. Kita, J. Appl. Phys. **115**, 17A719 (2014).
[7] H. Yanagihara, K. Uwabo, M. Minagawa, E. Kita, N. Hirota, J. Appl. Phys. **109**, 07C122 (2011).
[8] G. Dascalu, G. Pompilian, B. Chazallon, O. F. Caltun, S. Gurlui, C. Focsa, Appl. Surf. Sci. **278**, 38 (2013).
[9] G. Dascalu, G. Pompilian, B. Chazallon, V. Nica, O.bF. Caltun, S. Gurlui, C. Focsa, Appl. Phys. A. **110**, 915 (2012).
[10] D. Mukherjee, M. Hordagoda, R. Hyde, N. Bingham, H. Srikanth, S. Witanachchi, P. Mukherjee, ACS Appl. Mater. Interfaces. **5**, 7450 (2013).
[11] G. Dascalu, T. Popescu, M. Feder, O.F. Caltun, J. Magn. Magn. Mater. **333**, 69 (2013).
[12] D. Mukherjee, R. Hyde, M. Hordagoda, N. Bingham, H. Srikanth, S. Witanachchi, P. Mukherjee, J. Appl. Phys. **112**, 064101 (2012).
[13] C. Ursu, S. Gurlui, C. Focsa, G. Popa, Nucl. Instruments Methods Phys. Res. Sect. B Beam

Interact. with Mater. Atoms. **267**, 446 (2009).
[14] C. Ursu, O. G. Pompilian, S. Gurlui, P. Nica, M. Agop, M. Dudeck, C. Focsa, Appl. Phys. A. **101**, 153 (2010).
[15] C. Focsa, P. Nemec, M. Ziskind, C. Ursu, S. Gurlui, V. Nazabal, Appl. Surf. Sci. **255**, 5307 (2009).
[16] O. G. Pompilian, S. Gurlui, P. Nemec, V. Nazabal, M. Ziskind, C. Focsa, Appl. Surf. Sci. **278**, 352n(2013).
[17] L. Balika, C. Focsa, S. Gurlui, S. Pellerin, N. Pellerin, D. Pagnon, M. Dudeck, Spectrochim. Acta Part B At. Spectrosc. **74-75**, 184 (2012).
[18] S. Gurlui, M. Sanduloviciu, M. Strat, G. Strat, C. Mihesan, M. Ziskind, C. Focsa, J. Optoelectron. Adv. Mater. **8**, 148 (2006).
[19] S. Gurlui, M. Agop, P. Nica, M. Ziskind, C. Focsa, Phys. Rev. E. **78**, 026405 (2008).
[20] P. Nica, P. Vizureanu, M. Agop, S. Gurlui, C. Focsa, N. Forna, P. D. Ioannou, Z. Borsos, Jpn. J. Appl. Phys. 48 (2009).
[21] N. Bulgakova, A. Bulgakov, O. Bobrenok, Phys. Rev. E. **62**, 5624 (2000).
[22] D. B. Geohegan, A. A. Puretzky, Appl. Phys. Lett. **67**, 197 (1995).
[23] NIST Atomic Spectra Database, http://physics.nist.gov/PhysRefData/ASD/lines_form.html. (n.d.).
[24] Atomic spectral line database, http://www.cfa.harvard.edu/amp/ampdata/kurucz23/sekur.html. (n.d.).
[25] R. H. Huddlestone, S. L. Leonard, Plasma diagnostic technique, Academic press, New York (1965).
[26] G. Cristoforetti, A. De Giacomo, M. Dell'Aglio, S. Legnaioli, E. Tognoni, V. Palleschi, N. Omenetto, Spectrochim. Acta - Part B At. Spectrosc. **65**, 86 (2010).
[27] M. Salik, M. Hanif, J. Wang, X. Zhang, Int. J. Phys. Sci. **8**, 1738 (2013).
[28] A. De Giacomo, V. A. Shakhatov, O. De Pascale, Spectrochim. Acta - Part B **56**, 753 (2001).